Advanced Robotics

ISSN: 0169-1864 (Print) 1568-5535 (Online) Journal homepage: http://www.tandfonline.com/loi/tadr20

Multiobjective Optimization of 6-dof UPS Parallel Manipulators

Ridha Kelaiaia , Abdelouahab Zaatri & Olivier Company

To cite this article: Ridha Kelaiaia , Abdelouahab Zaatri & Olivier Company (2012) Multiobjective Optimization of 6-dof UPS Parallel Manipulators, Advanced Robotics, 26:16, 1885-1913, DOI: 10.1080/01691864.2012.703168

To link to this article: http://dx.doi.org/10.1080/01691864.2012.703168

Published online: 20 Jul 2012.

Taylor & Francis
Taylor & Francis Group

Advanced Robotics 26 (2012) 1885–1913

ADVANCED ROBOTICS
tandfonline.com/tadr

Full paper

Multiobjective Optimization of 6-dof UPS Parallel Manipulators

Ridha Kelaiaia[a,b]*, Abdelouahab Zaatri[c] and Olivier Company[b]

[a]Faculté de technologie, Université 20 Août 1955 Skikda, Bp 26 Route El hadaek, Skikda, Algérie; [b]The Montpellier Laboratory of Informatics, Robotics, and Microelectronics, UMR 5506 CNRS-UM2, 161 rue Ada, 34392 Montpellier Cedex 5, France; [c]Laboratory of Advanced Technology Applications, University of Constantine, Constantine, Algeria

Received 30 September 2011; accepted 31 December 2011

Abstract

The optimal design of parallel kinematic machines goes through two fundamental stages. The first one concerns the structural synthesis. It enables, a priori, to determine the choice of families of the most adapted architectures according to the desired applications such as flight simulators, machine-tools, medical applications, etc. This can be done by applying several techniques such as: screw theory, Lie groups, graph theory, finite element method, etc. The second one concerns the dimensional synthesis and aims to determine the dimensions of the architecture that has been selected during the structural synthesis. This stage remains a major task because the criteria of performance of a given architecture are strongly dependent on its sizing. In this paper, we present a dimensioning methodology of the architectural parameters of the 6-dof UPS (U: universal joint, P: prismatic joint, and S: ball-and-socket joint) parallel manipulators (the positions of the attachment points of the actuators on the base and mobile plate as well as the radius of the base and the mobile plate). The problem will be formulated as a multiobjective optimization problem (MOOP) by taking into account simultaneously several criteria of performance such as the workspace, kinetostatic performances, stiffness, and dynamic dexterity. The SPEA-II genetic algorithm is adopted to solve this type of MOOP.

Keywords

dimensioning methodology, multiobjective optimization, 6-dof UPS parallel manipulators, criteria of performance, genetic algorithm SPEA-II

1. Introduction

Parallel Kinematic Machines (PKMs) present some advantages that lead them to be used in various applications (assembly, handling, drilling, machining, etc.)

*To whom correspondence should be addressed. E-mail: ridakelaia@hotmail.com

DOI: 10.1080/01691864.2012.703168

[1,2]. If the design and optimization are done efficiently, this helps to provide a high structural stiffness and a good balance of forces between the chains. Another key factor is the possibility to put the actuators close to fixed frame to minimize moving masses. This results in a higher payload and low inertia. In spite the advantages of PKMs compared to conventional serial machines, their usability is still limited in the industry. This can be explained by the following reasons: Limitation of their workspace (ratio between machine footprint and usable workspace), singularities, which involve variability of the performances (workspace is not isotropic), complexity of the transformations between operational and joint spaces (the complexity of the forward geometrical models, which may not exist in analytical form), and difficulties for decoupling movements into translations and rotations. These previous issues represent fundamental problems for many researchers, which are interested in the design, optimization, and analysis of the PKMs. This paper addresses the architecture optimization of 6-dof UPS (U: universal joint, P: prismatic joint, and S: ball-and-socket joint) parallel manipulators. The design optimization is conducted on the basis of genetic algorithms-based multiobjective optimization concept.

2. A Multiobjective Optimization Problem

In our approach, the dimensional synthesis problem is considered as a multiobjective optimization problem (MOOP). Mathematically, this can be stated in the following form:

Find a vector $P^* = [P_1^*, P_2^*, ..., P_n^*]^T$
That **Minimizes/Maximizes** $F(P) = [f_1(P), f_2(P), \ldots, f_k(P)]^T$
With $g_m(P) \leq 0$ (m constraints of inequality)
and $h_l(P) = 0$ (l constraints of equality).
$P^* \in \mathbb{R}^n$: Vector of the decision variables.
$F(P^*) \in \mathbb{R}^k$: Vector of the objective functions.

2.1. Definition of Objective Functions

To formulate the mathematical model as a MOOP, we consider the objective functions such as dexterous workspace, kinetostatic performances, stiffness, and dynamic dexterity. Then, we will express each of them in the form of a mathematical function.

2.1.1. Workspace

The workspace W is one of the most important factors for designing PKMs. Theoretically, it is the set of space configurations that the end-effector can reach. This space is defined by its limits which are imposed by the joints (active and

passive), the lengths of segments, and by the internal collisions. Consequently, a well-conditioned subworkspace of the accessible workspace must be determined. Only the accessible points having a condition number of the Jacobian matrix lower than an imposed threshold will be retained to represent the subworkspace. This procedure allows the obtention of a dextrous workspace W_{dextrous} (all the locations of the operating point of the robot for which all orientations are possible), hence:

$$W_{\text{dextrous}} \rightarrow \max \tag{1}$$

2.1.2. *Kinetostatic Performances*

They are represented by the kinematic and static dexterity, which are defined by the ability of the PKM to transmit velocities and forces from the actuators to the end-effector. They can be used for the measurement of the:

- Precision with which the end-effector and contact forces can be controlled by joints forces at any direction within the workspace of the PKM.
- Proximity of a singular configuration.

These performances can be evaluated by means of the velocities and forces equations of PKM:

$$\begin{cases} \dot{\rho} = J^{-1}\dot{X} = J_{\rho}^{-1} J_x \dot{X} \\ f = J^{-T}\tau \end{cases} \tag{2}$$

where $|J_\rho| \neq 0$.

The inverse Jacobian matrix J^{-1} characterizes the quality of transformation between the actuators and the end-effector; it allows analyzing the kinematic and static dexterity of the PKM. The condition number of J^{-1} is used to measure the kinematic dexterity. It is defined by the ratio between the maximum and minimum singular values of J^{-1} which are, respectively, $\sigma_{\max}(J^{-1})$ and $\sigma_{\min}(J^{-1})$:

$$\kappa_J = \frac{\sigma_{\max}(J^{-1})}{\sigma_{\min}(J^{-1})} \in [1, \infty[\tag{3}$$

When the condition number κ_J tends to infinity, the inverse Jacobian matrix J^{-1} becomes a singular matrix. Physically, this means that the PKM is in a singular configuration, and when $\kappa_J = 1$, it becomes a perfectly conditioned matrix, in this case the configurations are called isotropic, it means that the velocities and the static stiffness of the end-effector are equal in all directions. In other words,

the PKM end-effector will have the same facility to move in all the directions, which is highly desirable. As this measure has only a local character (local property), a solution proposed by Gosselin and Angeles [4] is to integrate the dexterity over the workspace and to normalize by the volume $\int_W dW$ of the workspace. So, the objective function is given by:

$$\eta_J = \frac{\int_W \kappa_J dW}{\int_W dW} \rightarrow \min \tag{4}$$

where dW, represents an infinitesimal element of the workspace. η_J can be approximated by a discrete sum. So, the objective function becomes:

$$\eta_J = \frac{1}{\int_W} \sum_W \kappa_J \rightarrow \min \tag{5}$$

2.1.3. *Stiffness*

The value of the stiffness evolves according to the geometry, the topology of the structure, and the configuration (position and orientation) of the end-effector within its workspace. The stiffness of a PKM at a given point of its workspace can be characterized by its stiffness matrix. This matrix combines the forces and moments applied to the end-effector. In case where we take into account only the linear actuator stiffness (the other parts are considered as rigid bodies), the matrix of stiffness can be obtained using kinematic and static equations; a modification of the joint variable $\delta\rho$ corresponds to a variation of the joint force $\delta\tau$ [1] such as:

$$\delta\tau = k\ \delta\rho \tag{6}$$

$$\delta\rho = J^{-1}\ \delta X \tag{7}$$

$$\delta f = J^{-T}\ \delta\tau \tag{8}$$

If we replace (6) and (7) in (8), we found:

$$\delta f = k\, J^{-T}\, J^{-1}\ \delta X \tag{9}$$

The stiffness matrix K is given by:

$$K = k\, J^{-T}\, J^{-1} = k\ (J\, J^T)^{-1} \tag{10}$$

k is a scalar representing the stiffness of each of the actuators. The majority of the PKMs have similar kinematic chains ($k_1 = k_2 = \cdots = k_t = k$), this can reduce its costs. The improvement of stiffness can be made by the analysis of the matrix $(J^T)^{-1}$;, hence it is possible to estimate the minimum and maximum values of this stiffness, and by the calculation of the eigenvalues of the matrix $(J\,J^T)^{-1}$,, the small value corresponds to the minimum and the large one corresponds to the maximum of the stiffness. The goal here is to have best possible stiffness, this can be obtained by:

$$\lambda_{\min}((JJ^T)^{-1}) = (\sigma_{\min}(J^{-1}))^2 \rightarrow \max \;\Leftrightarrow\; \kappa_J \rightarrow \min \tag{11}$$

To characterize it over the manipulator workspace, we use the global index η_J given by relation (5).

2.1.4. Dynamic Dexterity

We mean by dynamic performances, the dynamic dexterity. For its measurement we use the index of dynamic isotropy. Generally, the mass matrix of PKMs can be obtained on the basis of their kinetic energy [5]. For a rigid segment, it can be written as follows:

$$T_i = \frac{1}{2}(m_i v_{Gi}^T v_{Gi} + w_{Gi}^T I_i w_{Gi}) \tag{12}$$

where $v_{Gi} = J_{v,i}\,\dot{\rho}$ and $w_{Gi} = J_{w,i}\,\dot{\rho}$.

v_{Gi} and w_{Gi}, translational and angular velocity of the center of gravity of the ith body; $J_{v,i}$ and $J_{w,i}$, Jacobian matrix of the translation and orientation of the ith body.

Consequently, the kinetic energy of the PKM is the sum of the kinematic energies of all segments of the PKM:

$$T = \sum_{i=1}^{n} T_i = \frac{1}{2}\,\dot{\rho}^T \left[\sum_{i=1}^{n}(m_i\,J_{v,i}^T\,J_{v,i} + J_{w,i}^T\,I_i\,J_{w,i})\right]\dot{\rho} \tag{13}$$

Hence, the mass matrix of the PKM is defined as:

$$M = J^{-T}\left(\sum_{i=1}^{n}(m_i\,J_{v,i}^T\,J_{v,i} + J_{w,i}^T\,I_i\,J_{w,i})\right)J^{-1} \tag{14}$$

The evaluation of the dynamic performances is made according to the concept of the generalized inertia ellipsoid proposed by Asada [6], which indicates that the movement of the end-effector is easy (bigger acceleration) in the direction of the main larger axis of this ellipsoid and more difficult (less accelerated) in the direction of the main small axis. It is strongly recommended to make the acceleration isotropic along all the directions in order to obtain a better dynamic dexterity. The condition number of the mass matrix $(M = J^{-T}I(q)J^{-1})$ noted κ_M is used here to measure this dexterity and is defined by:

$$\kappa_M = \frac{\sigma_{\max}(M)}{\sigma_{\min}(M)} \tag{15}$$

The dynamic dexterity as well as the kinematic dexterity depend on the configuration and the geometrical parameters of the PKM. It varies within the workspace. To describe it on the whole accessible workspace by the PKM, we use the global dynamic dexterity index η_M [7] which is defined by:

$$\eta_M = \frac{\int_W \kappa_M dW}{\int_W dW} \rightarrow min \tag{16}$$

η_M can be also approximated by a discrete sum. So, the objective function becomes:

$$\eta_M = \frac{1}{\int_W} \sum_W \kappa_M \rightarrow \min \tag{17}$$

2.2. Definition of the Constraints

2.2.1. Joints Limits

They are represented by the actuated and the passive joints:

$$\rho_t^{\min} \leq \rho_t \leq \rho_t^{\max} \tag{18}$$

$$\xi_v^{\min} \leq \xi_v \leq \xi_v^{\max} \tag{19}$$

where t, number of the actuated joints and v, number of passive joints.

2.2.2. Collisions Avoidance

Collisions avoidance guarantees the orientation aptitude of PKM. If we denote by R_j, R_{j+1} the radius of two cylindrical segments and A_jB_j, $A_{j+1}B_{j+1}$ (Fig. 1),

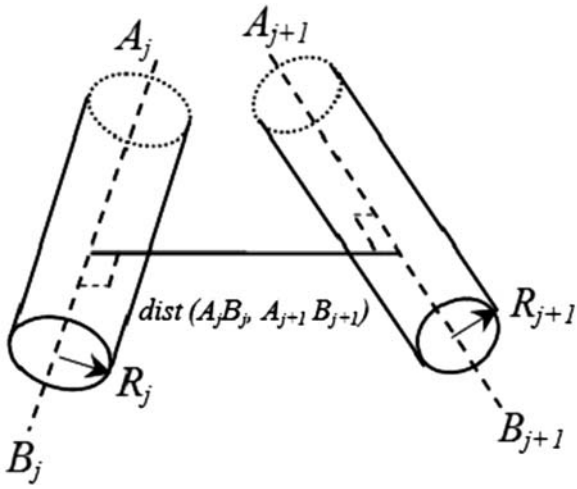

Figure 1. Distance between two segments.

we can ensure that there is no mechanical interference if the distance between any segments pair verifies the following condition:

$$dist(A_jB_j, A_{j+1}B_{j+1}) \geq R_j + R_{j+1} \tag{20}$$

2.2.3. *Technological Constraints*

They include constraints such as actuators strokes, geometrical dimensions of the end-effector and the PKM emplacement of in a chain of machining (e.g. assembly), the bulk of the machine, etc.

2.3. *Mathematical Formulation of the Problem*

The formulation of the problem of the optimal design based on the multiobjective optimization has a role to find the best dimensions of geometrical parameters of the PKM, which guarantees the best performances while satisfying the geometrical and technological constraints.

After analyzing the various performances criteria and their associated objective functions, we established that they can be classified and represented as follows:

- Dextrous workspace, kinetostatic performances, and stiffness are represented by the relation (5).
- Dynamic dexterity is represented by the relation (15).

Finally, the problem of the multiobjective optimization is formulated as follows:

Find a vector P^* (vector of the variables of design) that:

$$\min\ F(P) = \min \begin{bmatrix} f_1 = \eta_J \\ f_2 = \eta_M \end{bmatrix} \tag{21}$$

Subject to:

$$\begin{cases} \rho_t^{\min} \le \rho_t \le \rho_t^{\max} \\ \xi_v^{\min} \le \xi_v \le \xi_v^{\max} \\ \text{dist}(A_jB_j, A_{j+1}B_{j+1}) \ge R_j + R_{j+1} \\ \text{Other constraints related to the studied PKM} \end{cases} \tag{22}$$

2.4. Resolution Approaches

There are several techniques for solving this problem; the more usual consists in treating successively the objectives. The result gives advantage to extreme solutions. Other techniques consist in transforming the MOOP into a monoobjective optimization problem, for which there exist various methods (the goal attainment, method of compromise, etc.). The simplest is the method of weighted sum of objective functions. Its principle is to apply a weighting coefficient to each objective function and then to take the sum of a weighted objective functions. Hence, we obtain a new, unique objective function. Nevertheless, these methods cannot discover solutions hidden in concavities and in some structural optimization problems it can behave catastrophically [8].

The appearance of new kind of methods, called metaheuristics, which include the simulated annealing method, ant colony algorithms, tabu search and genetic algorithms, etc. overcomes the problems encountered with the conventional methods. In our case, we opted for genetic algorithms due to their good adequacy with our problem; they offer several advantages such as overcoming the obstacle of the local minima (or maxima) and enabling to obtention of the optimal Pareto front of a MOOP. Among these algorithms, we propose to use the SPEA-II (Strength Pareto Evolutionary Algorithm, see appendix B for more details) [9], it determines optimal Pareto fronts.

3. Case Study: 6-dof UPS Parallel Manipulators

Our objective is to optimize the vector of the geometrical parameters (Fig. 3), which is composed of:

- Radius of the base r_b.
- Radius of the mobile plate r_p.

- The positions of the attachment points of the actuators on the base defined by r_b and α_i:

$$^{b}B_i = \begin{bmatrix} r_b \cos(\alpha_i) \\ r_b \sin(\alpha_i) \\ 0 \end{bmatrix} \quad i = 1, \ldots, 6 \tag{23}$$

- The positions of the attachment points of the actuators on the mobile plate defined by r_p and β_i:

$$^{n}P_i = \begin{bmatrix} r_p \cos(\beta_i) \\ r_p \sin(\beta_i) \\ 0 \end{bmatrix} \quad i = 1, \ldots, 6 \tag{24}$$

To do this, we will determine the geometrical and kinematics models and the mass matrix of the 6-dof UPS parallel manipulators.

3.1. Description of the 6-dof UPS Parallel Manipulators

The 6-dof UPS parallel manipulators [10] are composed of the fixed base and mobile plate supposed perfectly rigid (Fig. 2). They are connected by six links of variable length ρ_i ($i = 1, \ldots, 6$) articulated with a universal joint at the B_i points and with ball-and-socket joints at the P_i points on the mobile plate. The reference frame $\{R_b\}$:$(O_b - x_b, y_b, z_b)$ is set up at the center of the base. The reference frame $\{R_n\}$:$(O_n - x_n, y_n, z_n)$ is attached to the center of mobile plate.

The position of the origin O_n of the moving frame in a reference frame $\{R_b\}$ attached to the base is given by the position vector $^{b}r = [x, y, z]^T$, and its orientation by the rotation matrix R relating the components of a moving frame $\{R_n\}$ attached to the mobile plate with respect to the reference frame $\{R_b\}$. It is defined by the angles Roll-Pitch-Yaw.

3.2. Inverse Geometrical Model

The kinematic model of this PKM enables to determinate the links lengths ρ_i for a given configuration (position and orientation) of the mobile plate. To solve this problem, we use the following relation:

$$\overrightarrow{B_iP_i} = \overrightarrow{B_iO_b} + \overrightarrow{O_bO_n} + \overrightarrow{O_nP_i} \tag{25}$$

The projection of the Equation (25) in the reference frame related to the base $\{R_b\}$ gives:

$$\rho_i \eta_i = -\,^{b}B_i + \,^{b}r + R\,^{n}P_i \tag{26}$$

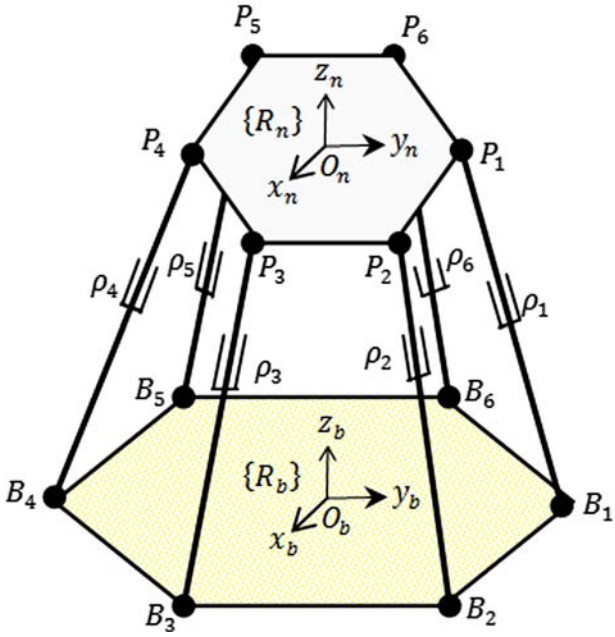

Figure 2. Platform of Gough–Stewart.

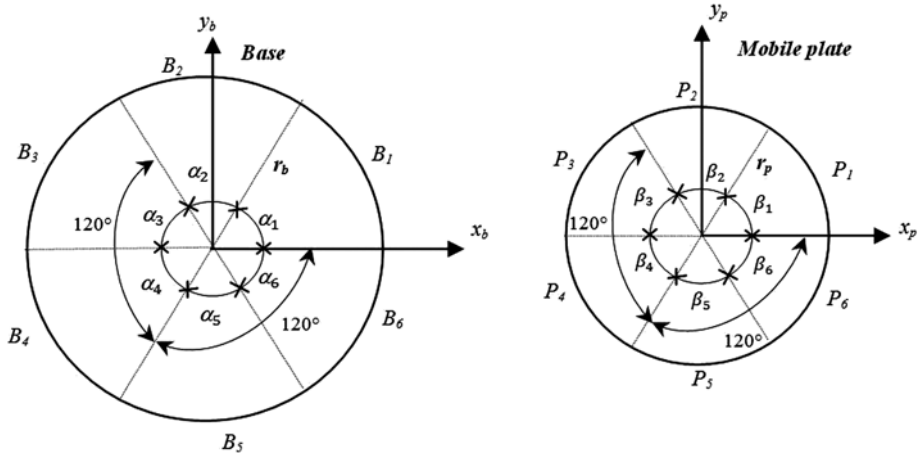

Figure 3. Parameterization of the 6-dof UPS parallel manipulators.

$\vec{\eta}_i = \frac{\overrightarrow{B_iP_i}}{\rho_i}$, the unit vector associated to link i and ρ_i, length of link i (actuated joint coordinate of link i), it is given by:

$$\rho_i^2 = \| \overrightarrow{B_iP_i} \|^2 \tag{27}$$

R: rotation matrix from the moving frame to the reference frame defined by the angles Roll-Pitch-Yaw:

$$^{b}R_{p} = R_{x,\psi}\, R_{y,\theta}\, R_{z,\phi} = \begin{bmatrix} c\phi\, c\theta & c\phi\, s\theta\, s\psi - s\phi\, c\psi & c\phi\, s\theta\, c\psi + s\phi\, s\psi \\ s\phi\, c\theta & s\phi\, s\theta\, s\psi + c\phi\, c\psi & s\phi\, s\theta\, c\psi - c\phi\, s\psi \\ -s\theta & c\theta\, s\psi & c\theta\, c\psi \end{bmatrix} \quad (28)$$

where $R_{x,\psi} = \begin{bmatrix} 1 & 0 & 0 \\ 0 & c\psi & -s\psi \\ 0 & s\psi & c\psi \end{bmatrix}$, $R_{y,\theta} = \begin{bmatrix} c\theta & 0 & s\theta \\ 0 & 1 & 0 \\ -s\theta & 0 & c\theta \end{bmatrix}$, $R_{z,\phi} = \begin{bmatrix} c\phi & -s\phi & 0 \\ s\phi & c\phi & 0 \\ 0 & 0 & 1 \end{bmatrix}$, $s : sin$, and $c : cos$

3.3. Direct Kinematic model

The direct kinematic model is essential for the process of optimization; it is obtained by the resolution of a system of nonlinear equations using the iterative method of Newton [11]:

3.4. Jacobian Matrix

We design by J^{-1} the inverse Jacobian matrix, which relates the velocities of the segments to the linear and angular velocities of the mobile plate, we have:

$$\frac{d(\overrightarrow{O_bP_i})}{dt} = \frac{d(\overrightarrow{O_bO_n})}{dt} + \overrightarrow{P_iO_n} \wedge \overrightarrow{\Omega} \quad (29)$$

The projection of (29) on the reference frame $\{R_b\}$ gives:

$$\frac{d(\overrightarrow{O_bP_i})}{dt} = \overrightarrow{^{b}\dot{r}} + R\ \overrightarrow{P_iO_n} \wedge \overrightarrow{\Omega} \quad (30)$$

where

$$\frac{d\rho_i}{dt} = \frac{d(\overrightarrow{O_bP_i})}{dt}\ \overrightarrow{\eta_i} = (\overrightarrow{^{b}\dot{r}} + R\ \overrightarrow{P_iO_n} \wedge \overrightarrow{\Omega}) \cdot \overrightarrow{\eta_i} \quad (31)$$

By taking into account the relation: $\overrightarrow{u}(\overrightarrow{v} \wedge \overrightarrow{w}) = \overrightarrow{w}(\overrightarrow{u} \wedge \overrightarrow{v})$, we get:

$$\frac{d\rho_i}{dt} = \overrightarrow{\eta_i}\ \overrightarrow{^{b}\dot{r}} + (R\ \overrightarrow{O_nP_i} \wedge \overrightarrow{\eta_i}).\ \overrightarrow{\Omega} \quad (32)$$

$$\dot{\rho}_i = J^{-1}\dot{X} \tag{33}$$

with:

$$J^{-1} = \begin{bmatrix} \eta_1^T & \dots & (R\,{}^nP_1 \wedge \eta_1)^T \\ \vdots & \ddots & \vdots \\ \eta_6^T & \dots & (R\,{}^nP_6 \wedge \eta_6)^T \end{bmatrix} \tag{34}$$

where $\dot{X} = [{}^b\dot{r}^T\ \Omega^T]^T$ and $\dot{\rho}_i = \frac{d\rho_i}{dt} = [\dot{\rho}_1, \dots, \dot{\rho}_6]^T$. ${}^b\dot{r} = [\dot{x}\ \dot{y}\ \dot{z}]^T$, linear velocity of the mobile plate and Ω, angular velocity of the mobile plate.

3.5. Homogenization of the Jacobian Matrix

In case where the Jacobian matrix is composed of two Jacobian submatrices, with elements expressed by different units, i.e. the task carried out by the PKMs is defined in position and orientation. As a direct consequence, the condition number does not have a physical sense. To resolve this problem (the inconsistency of physical units), several proposals have been made by the researchers [12]. In our case, we use the method proposed by Fassi et al. [13] to find the characteristic length. It is given by:

$$L_c = \sqrt{\frac{\text{trace}(J_2^T J_2)}{\text{trace}(J_1^T J_1)}} \tag{35}$$

where $J^{-1} = [J_1,\ J_2]$ and $J_1,\ J_2$ are two submatrices of dimensions 6×3.

3.6. Singularity Analysis

Several methods [1] (geometrical, algebraic, etc.) are used to determine the singular configurations. In this work, the method based on the determination of the roots of the determinant of the PKM Jacobian matrix is employed to find these configurations. As a result, we distinguish the following cases: $|J_x| = 0$: it corresponds to the appearance of uncontrollable mobility of the end-effector, because it is possible to move it whereas the actuated joints are blocked. These singularities can exist inside the reachable workspace of the PKM. In these configurations, the PKM gains one or more degree (s) of freedom. $|J_\rho| = 0$: it is not possible to generate certain velocities of the end-effector in certain directions. These singularities represent the limits of the reachable workspace. In these configurations, the PKM loses one or more degree(s) of freedom. $|J_x| = 0$ and $|J_\rho| = 0$: the mobile plate can move whereas the actuators are blocked and reciprocally. In the case of Gough–Stewart platform, the reader can see the study in [14] for more details.

3.7. Evaluation of the Mass Matrix of the System

The kinetic energy of the system is the sum of the kinetic energy of the six actuators (segments) and the kinetic energy of the mobile plate (see the appendix for more details). It is given by:

$$T = T_p + \sum_{i=1}^{6} T_{s,i} = \frac{1}{2}\,\dot{\rho}^T (J^T \begin{bmatrix} M_p & 0 \\ 0 & I_p \end{bmatrix} J + I_a)\,\dot{\rho} \tag{36}$$

$$I_s = J^T \begin{bmatrix} M_p & 0 \\ 0 & I_p \end{bmatrix} J \; + \; I_a \tag{37}$$

where $T_{s,i}$, kinetic energy of the ith actuator; T_p, kinetic energy of the mobile plate; I_a, the inertia matrix of the six actuators; m, mass of the mobile plate; I_p, tensor of inertia of the mobile plate; and $M_p = diag(m, m, m)$. Hence the inertia matrix of the system is given by:

$$M = J^{-T} I_s J^{-1} \tag{38}$$

3.8. Formulation of the Optimization Problem

$$\begin{cases} \text{Find a vector } P^* \text{ that :} \\ \qquad \min\ F(P) = min \begin{bmatrix} f_1 = \eta_J \\ f_2 = \eta_M \end{bmatrix} \\ \text{Subject to :} \\ \qquad 660 \le \rho_i(mm) \le 1091 \\ \qquad \text{dist}(A_jB_j, A_{j+1}B_{j+1}) \ge 90 \text{ mm} \\ \qquad \frac{-\pi}{9} \le \psi \text{ (Angle Roll)} \le \frac{\pi}{9} \\ \qquad \frac{-\pi}{18} \le \theta \text{ (Angle Pitch)} \le \frac{\pi}{18} \\ \qquad \frac{-\pi}{18} \le \phi \text{ (Angle Yaw)} \le \frac{\pi}{18} \\ \qquad m(\text{mass of the mobile plate + charge}) = 100 \text{ kg} \\ \qquad m_{\text{pis},i}(\text{mass of the piston of each actuator}) = 12 \text{ kg} \\ \qquad m_{\text{cyl},i}(\text{mass of the cylinder of each actuator}) = 18 \text{ kg} \\ \qquad I_{xx} = I_{yy} = I_{zz} = 36 \text{ kg m}^2 \\ \qquad \text{For all } i = 1, \ldots, 6 \text{ and } j = 1, \ldots, 5 \end{cases} \tag{39}$$

3.9. Results and Discussion

Figure 3 represents the parameterization of the 6-dof UPS parallel manipulators where the positions of the attachment points of the actuators on the base are represented by $B_1, B_2, B_3, B_4, B_5, B_6$. These points are separated by the angles $\alpha_1, \alpha_2, \alpha_3, \alpha_4, \alpha_5, \alpha_6$. On the other hand, the positions of the attachment points of the actuators on the mobile plate are represented by $P_1, P_2, P_3, P_4, P_5, P_6$. They are separated by the angles $\beta_1, \beta_2, \beta_3, \beta_4, \beta_5, \beta_6$. With the parameterization corresponding to this structure, the collision avoidance is taken into account. As a result, the vector P^* (the vector of the variables of design) corresponding to the optimal value of the objective functions is given by: $P^* = [r_b, \alpha_1, \alpha_2, \alpha_3, \alpha_4, \alpha_5, \alpha_6, r_b, \beta_1, \beta_2, \beta_3, \beta_4, \beta_5, \beta_6]^T$.

With respect to the delimitation of the angles α_i and β_i, we can distinguish three cases of parameterization. Three cases lead to three remarkable architectures which are namely simplified symmetric manipulator (SSM), triangular simplified symmetric manipulator (TSSM) and the minimal simplified symmetric manipulator (MSSM) [1]. These architectures will be compared to each other thereafter.

3.9.1. First Case

For this case, the intervals of variation of the angles α_i are expressed by:

$$\alpha_i \in \left[(i-1)\frac{\pi}{3},\ i\frac{\pi}{3}\right] \quad \text{and} \quad \beta_i \in \left[(i-1)\frac{\pi}{3},\ i\frac{\pi}{3}\right],\ i = 1, \ldots, 6$$

We notice that for the base, every two points converge into a single common point as well. Finally, we get three points. This remark holds for the base and the mobile plate. The optimized vector P_1^* of geometrical parameters chosen from the Pareto front (Fig. 10) is:

$$\begin{aligned} P_1^* &= [r_b, \alpha_1, \alpha_2, \alpha_3, \alpha_4, \alpha_5, \alpha_6, r_b, \beta_1, \beta_2, \beta_3, \beta_4, \beta_5, \beta_6]^T \\ &= \left[0.450\ \text{m}, \frac{\pi}{3}, \frac{\pi}{3}, \pi, \pi, \frac{5\pi}{3}, \frac{5\pi}{3}, 0.240\ \text{m}, 0, \frac{2\pi}{3}, \frac{2\pi}{3}, \frac{4\pi}{3}, \frac{4\pi}{3}, 2\pi\right]^T \end{aligned}$$

Figures 4 and 5 represent the 6-dof UPS parallel manipulators obtained by considering the vector P_1^*. For the base, we precisely notice that each pair of attachment points (B_1, B_2), (B_3, B_4), and (B_5, B_6) converge into a single common point. For the mobile plate, we also notice that each pair of attachment points

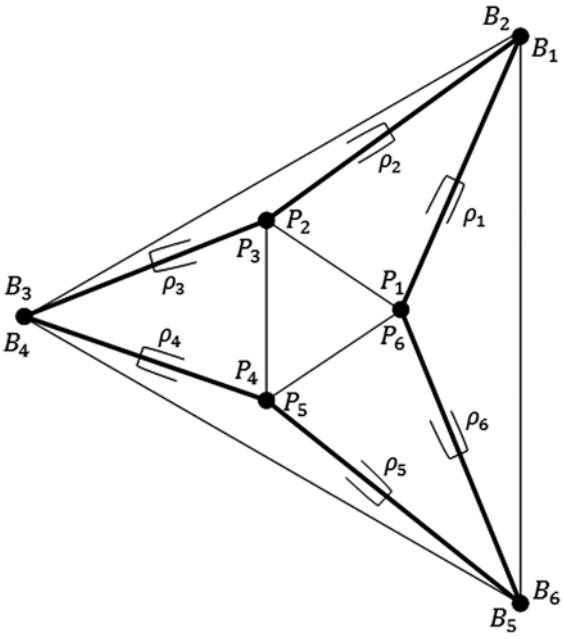

Figure 4. Representation of the attachment points with the first case.

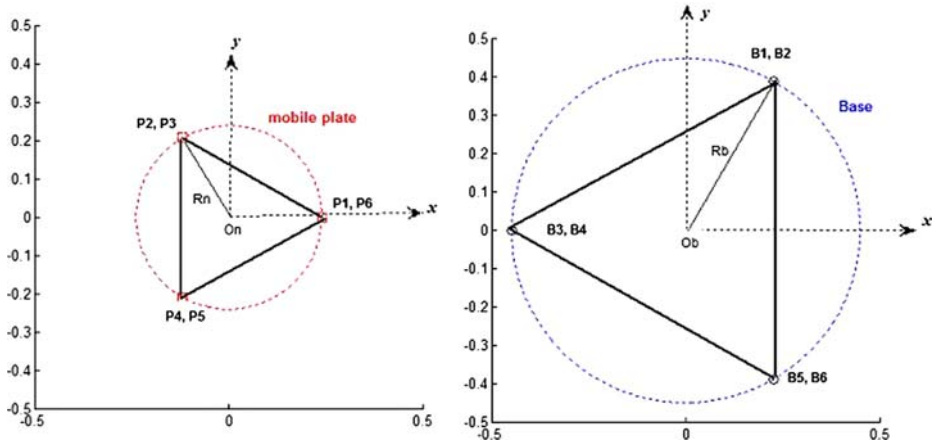

Figure 5. The positions of the attachment points of the actuators on the mobile plate and on the base.

(P_1, P_6), (P_2, P_3), and (P_4, P_5) converge into a single common point. The obtained architecture represents the MSSM which has a triangular base and a triangular mobile plate.

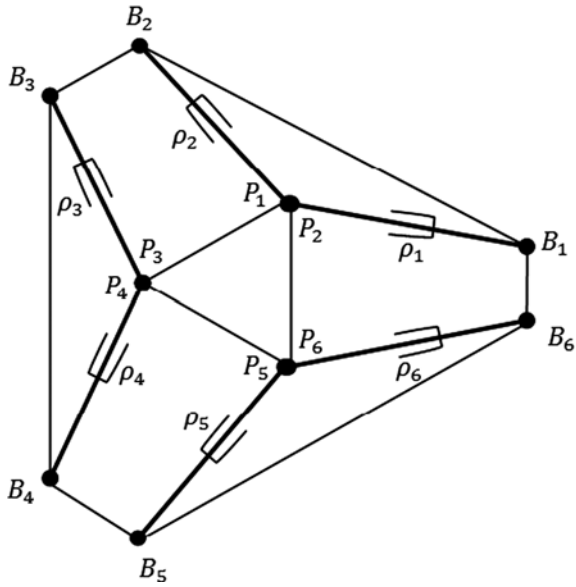

Figure 6. Representation of the attachment points with the second case.

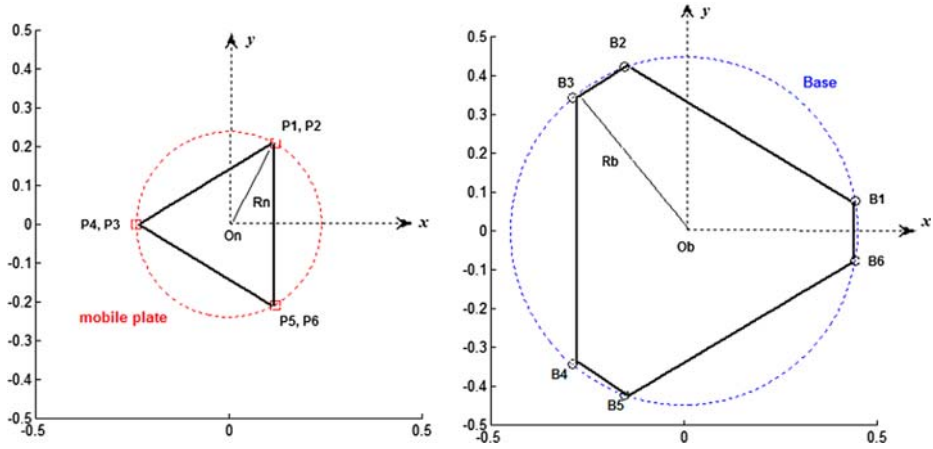

Figure 7. The positions of the attachment points of the actuators on the mobile plate and on the base.

3.9.2. Second Case

To avoid the architecture of type 1 (the first case), we limit the interval of variation of the angles α_i. This necessarily leads to an hexagonal form for the base. The intervals are chosen as follows:

$$\alpha_i \in \left[(i-1)\frac{\pi}{3}+\frac{\pi}{18},\ i\frac{\pi}{3}-\frac{\pi}{18}\right] \quad \text{and} \quad \beta_i \in \left[(i-1)\frac{\pi}{3},\ i\frac{\pi}{3}\right],\ i=1,\ldots,6$$

The optimized vector P_2^* of geometrical parameters chosen from the Pareto front (Fig. 10) is

$$\begin{aligned} P_2^* &= [r_b, \alpha_1, \alpha_2, \alpha_3, \alpha_4, \alpha_5, \alpha_6, r_b, \beta_1, \beta_2, \beta_3, \beta_4, \beta_5, \beta_6]^T \\ &= \left[0.450\text{ m}, \frac{\pi}{18}, \frac{11\pi}{18}, \frac{13\pi}{18}, \frac{23\pi}{18}, \frac{25\pi}{18}, \frac{35\pi}{18}, 0.240\text{ m}, \frac{\pi}{3}, \frac{\pi}{3}, \pi, \pi, \frac{5\pi}{3}, \frac{5\pi}{3}\right]^T \end{aligned}$$

Figures 6 and 7 represent the 6-dof UPS parallel manipulators obtained by considering the vector P_2^*. For the mobile plate, we notice that each pair of attachment points $(P_1, P_2), (P_3, P_4)$, and (P_5, P_6) converge into a single common point. The obtained architecture represents the TSSM, which has typically an hexagonal base and a triangular mobile plate.

3.9.3. Third Case

To avoid the architectures of the first and the second cases, we limit the interval of variation of the angles α_i and β_i. This necessarily leads to an hexagonal form for the base and the mobile plate. The intervals are chosen as follows:

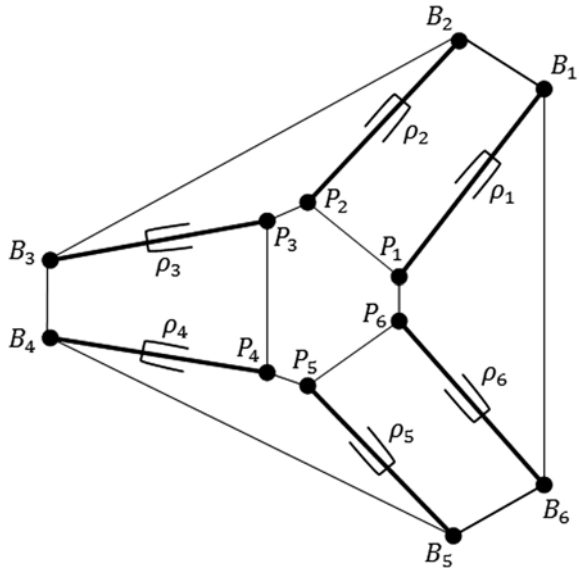

Figure 8. Representation of the attachment points with the third case.

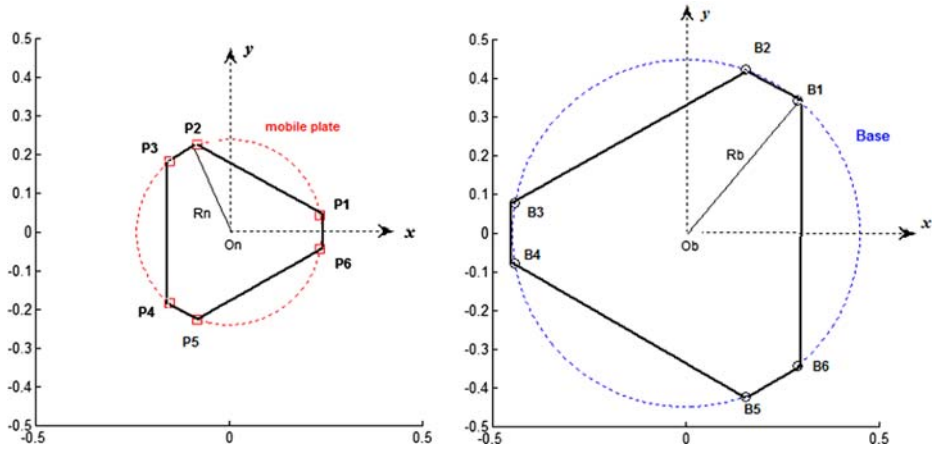

Figure 9. The positions of the attachment points of the actuators on the mobile plate and on the base.

$$\alpha_i \in \left[(i-1)\frac{\pi}{3}+\frac{\pi}{18},\ i\frac{\pi}{3}-\frac{\pi}{18}\right] \quad \text{and}$$
$$\beta_i \in \left[(i-1)\frac{\pi}{3}+\frac{\pi}{18},\ i\frac{\pi}{3}-\frac{\pi}{18}\right],\ i=1,\ldots,6$$

The optimized vector P_3^* of geometrical parameters chosen from the Pareto front (Fig. 10) is:

$$P_3^* = [r_b, \alpha_1, \alpha_2, \alpha_3, \alpha_4, \alpha_5, \alpha_6, r_b, \beta_1, \beta_2, \beta_3, \beta_4, \beta_5, \beta_6]^T$$
$$= \left[0.450\ \text{m}, \frac{5\pi}{18}, \frac{7\pi}{18}, \frac{17\pi}{18}, \frac{19\pi}{18}, \frac{29\pi}{18}, \frac{31\pi}{18}, 0.240\ \text{m}, \frac{\pi}{18}, \frac{11\pi}{18}, \frac{13\pi}{18}, \frac{23\pi}{18}, \frac{25\pi}{18}, \frac{35\pi}{18}\right]^T$$

Figures 8 and 9 represent the 6-dof UPS parallel manipulators obtained by considering the vector P_3^*. The obtained architecture represents the SSM, which has typically an hexagonal base and an hexagonal mobile plate.

3.10. Comparison Between the Obtained Architectures

By applying the proposed methodology and by solving the MOOP (see Equation (39)) corresponding to the three cases of configurations, we get Fig. 10, which represents the three Pareto fronts of the three parameterizations, it shows that the best compromise corresponds to the first parameterization (first case) which is the MSSM. As the profiles of the Pareto fronts are almost similar (Fig. 10), we can classify them according to the optimality of the objective functions. The best choice corresponds to the first case (MSSM), then the second case (TSSM), and finally the third case (SSM).

3.11. Comparison with Other Results

In order to evaluate our methodology, we compared it with the results given by Gao et al. [16] and Lou et al. [17]. In [16], the others have used a multiobjective optimization for 6-dof parallel robot by considering the system stiffness and dexterity as objective functions. They used an optimization method based on artificial intelligence (the neural network-based standard back-propagation learning algorithm and the Levenberg–Marquardt algorithm) for solving the problem. They converted the MOOP into single objective optimizatipProblem (SOOP) by distributing the weighting factors of different objective function values (the

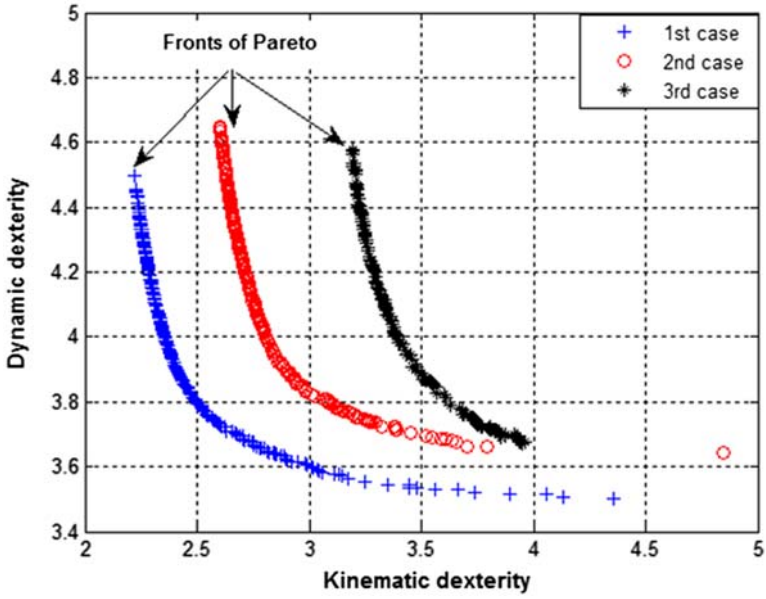

Figure 10. Fronts of Pareto.

Table 1.
Comparison with other results

Parameters	$r_b(m)$	α_1	α_2	α_3	α_4	α_5	α_6
Base							
Results obtained by Gao et al. [16]	0.20928	18°	102°	138°	222°	268°	−18°
Results obtained by Lou et al. [17]	0.6153	0°	0°	120°	120°	240°	240°
Our results	0.4500	60°	60°	180°	180°	300°	300°
	$r_p(m)$	β_1	β_2	β_3	β_4	β_5	β_6
Mobile plate							
Results obtained by Gao et al. [16]	0.10	48°	72°	168°	192°	288°	−48°
Results obtained by Lou et al. [17]	0.0631	−60°	60°	60°	180°	180°	−60°
Our results	0.2400	0°	120°	120°	240°	240°	0°

weighted sum of objective functions method). Nevertheless, this conversion presents some drawbacks. It cannot find solutions, which can be hidden in concavities. This means that without convexity assumption, one cannot always obtain all efficient solutions by changing the value of weighting factors [8].

In the same context, Lou et al. [17] used the ε-constraint approach for solving the problem of dimensional design of the Gough–Stewart platform. In his approach, there is no aggregation of objectives (criteria). Only one of the original objectives is minimized and the others are transformed to constraints (ε). The author has used the effective regular workspace as the main objective function and he transformed the others criteria (orientation and position dexterity) into inequality constraints. Nevertheless, the problem with this approach is the suitable selection of ε to ensure a feasible solution. A further drawback of this method is that the use of severe constraints is rarely adequate for expressing true design objectives [8]. By applying the results presented in Table 1 and by considering the dexterity among others criteria. We notice as well as in [17] that the best architecture is the MSSM. Table 1 represents the results obtained by Gao et al. [16] and Lou et al. [17] and our results.

Though the results presented in the table are not obtained in the same conditions (actuators strokes), they allows us to have a general idea about the robustness of each approach.

If we take the kinematic dexterity as one of the criteria. We notice by comparing our results with the obtained results of [17] that the MSSM architecture is better than the other architectures (SSM and TSSM). However, the results obtained by Gao et al. [16] are not very precise, this is due to the method employed for solving the optimization problem (the weighted sum of objective functions method). Indeed, it does not guarantee optimal results. On the other hand, our approach guarantees optimal results because it overcomes the problems with the local minima (maxima).

4. Conclusion

In this paper, we presented a methodology of dimensional design of 6-dof UPS parallel manipulators based on a multiobjective optimization approach by means of genetic algorithms. We discussed and introduced several criteria (indices) of performance that enter in the dimensioning of PKMs such as the workspace, the kinetostatic performances, the stiffness, and the dynamic dexterity. Then, we formulated the MOOP by defining the objective functions from the criteria of performance, the constraints, and the variables of decision (geometrical parameters). We chose souhaitable algorithm to solve the problem, which is the SPEA-II.

To test the effectiveness of this methodology, we applied it to 6-dof UPS parallel manipulators for determining the geometrical parameters (the positions of the attachment points of the actuators on the base and mobile plate as well as their radius). Three types of geometrical parameterization of the 6-dof UPS

parallel manipulators have been proposed. For each case, we obtained an optimized vector of architectural parameters from the Pareto front. Comparing the three obtained architectures, we noticed that the best compromise corresponds to the MSSM architecture. Taking into account the generic approach followed in this problem and based on the obtained results, future work concerns the generalization of the design methodology to other PKMs with more complex architectures.

Notations

W	reachable workspace
X	generalized of the PKM
ρ	actuated joints variables
ξ	passives joints variables
$\dot{\rho}$	joints velocities
$\dot{X}$	velocity vector of the end-effector
J	Jacobian matrix
J^{-1}	inverse Jacobian matrix
J_x and J_ρ	two Jacobian submatrices
J_ρ^{-1}	inverse of J_ρ
$J_{v,i}$	Jacobian matrix of the translation of the ith body
$J_{w,i}$	Jacobian matrix of the orientation of the ith body
$\sigma_{max}(J^{-1})$	the maximum singular value of J^{-1}
$\sigma_{min}(J^{-1})$	the minimum singular value of J^{-1}
κ_J	condition number of the matrix J^{-1}
η_J	index of global kinematic dexterity
L_c	characteristic length
τ	actuated joint force/torque
f	force/torque vector applied to the end-effector
$\delta\rho$ and δX :	infinitesimal displacements
k	stiffness of each of the actuators
K	stiffness matrix
M	global inertia matrix of the PKM
k_M	condition number of the mass matrix M
η_M	index of global dynamic dexterity
v_{G_i}	translational velocity of the center of gravity of the ith body
w_{G_i}	angular velocity of the center of gravity of the ith body
dof	degrees of freedom
U	universal joint
P	prismatic joint
S	ball-and-socket joint
PKMs	Parallel Kinematic Machines
MOOP	Multiobjective Optimization Problem
SOOP	Single Objective Optimization Problem

References

1. J.-P. Merlet, *Parallel Robots*, 2nd ed., Springer, Heidelberg, Germany (2006).

2. J.-P. Merlet, Parallel manipulators: state of the art and perspectives, *Adv. Robotics* **8**(6), 535–544 (1994).
3. O. Company and F. Pierrot, Modelling and design issues of a 3-axis parallel machine-tools, *Mechanism and Machine Theory* **37**, 1325–1345 (2002).
4. C. Gosselin and J. Angeles, A Global performance index for the kinematic optimization of robotic manipulators, *J. Mech. Design* **113**, 220–226 (1991).
5. A. Codourey, Dynamic modeling of parallel robots for computed-torque control implementation, *Int. J. Robotic Res.* **17**(2), 1325–1336 (1998).
6. H. Asada, A geometrical representation of manipulator dynamics and its application to arm design, *ASME J. Dynam. Syst. Measure. Control* **105**, 131–135, 142 (1983).
7. J. Wu, J. Wang, T. Li, L. Wang and L. Guan, Dynamic dexterity of a planar 2-DOF parallel manipulator in a hybrid machine tool, *Robotica* **26**, 93–98 (2008).
8. Y. Collette and P. Siarry, *Multiobjective Optimization: Principles and Case Studies*, Springer, Berlin (2004).
9. E. Zitzler, M.Laumanns and L.Thiele, Spea2: improving the strength pareto evolutionary algorithm, *Technical Report 103, Computer Engineering and Networks Laboratory (TIK)*, ETH Zurich, Switzerland (2001).
10. D. Stewart, A platform with six degrees of freedom, *Proc. Inst. Mech. Eng.* **180**(5), 371–386, part 1 (1965).
11. J.-P. Merlet, Direct kinematics of parallel manipulators, *IEEE Trans. Robotics Automat.* **9**(6), 842–846, ISSN 1042–296X (1993).
12. J. Angeles, *Fundamentals of Robotic Mechanical Systems: Theory, Methods, and Algorithms*, 2nd ed., Springer, Verlag, Heidelberg, Germany (2003).
13. I. Fassi, G. Legnani and D. Tosi, Geometrical conditions for the design of partial or full isotropic hexapods, *J. Robotic Syst.* **22**(10), 507–518 (2005).
14. B. M. St-Onge and C. Gosselin, Singularity analysis and representation of the general Gough–Stewart platform, *Int. J. Robotics Res.* **19**(3), 271–288 (2000).
15. J. Lin and C.-W. Chen, Computer-aided-symbolic dynamic modeling for Stewart-platform manipulator, *Robotica* **27**, 331–341 (2009).
16. Z. Gao, D. Zhang and Y. Ge, Design optimization of a spatial six degree-of-freedom parallel manipulator based on artificial intelligence approaches, *Robotics Comput. Int. Manuf.* **26**, 180–189 (2010).
17. Y. Lou, G. Liu and Z. Li, Randomized optimal design of parallel manipulators, *IEEE Trans. Automat. Sci. Eng.* **5**(2), (2008).

Appendix A. Evaluation of the Mass Matrix of the System

The kinetic energy of the system is the sum of the kinetic energy of the six actuators (segments) and the kinetic energy of the mobile plate.

Calculation of the kinetic energy of an actuator i

The actuator (Fig. 11) is composed of two parts [15]: the cylinder represents the fixed part and the piston represents the moving part.

Calculation of the kinetic energy of each piston

$$T_{\text{pis},i} = \frac{1}{2}\,\overrightarrow{v_{G2i}^{T}}\, m_{\text{pis},i}\,\overrightarrow{v_{G2i}} + \frac{1}{2}\,\overrightarrow{w_{a,i}^{T}}\, I_{\text{pis},i}\,\overrightarrow{w_{a,i}} \tag{40}$$

v_{G2i}^{T}: translation velocity of the center of gravity of the piston;
$I_{pis,i}$: moment of inertia of the piston; and $m_{pis,i}$: mass of the piston.

- Calculation of v_{G2i}^{T}

$$\overrightarrow{B_iG_{2i}} = (\rho_i - l_{i2})\,\overrightarrow{\eta_i} \tag{41}$$

$$\overrightarrow{v_{G2i}} = \frac{d(\overrightarrow{B_iG_{2i}})}{dt} = \frac{d(\overrightarrow{B_iP_i})}{dt} - l_{i2}\frac{d\,\overrightarrow{\eta_i}}{dt} \tag{42}$$

with:

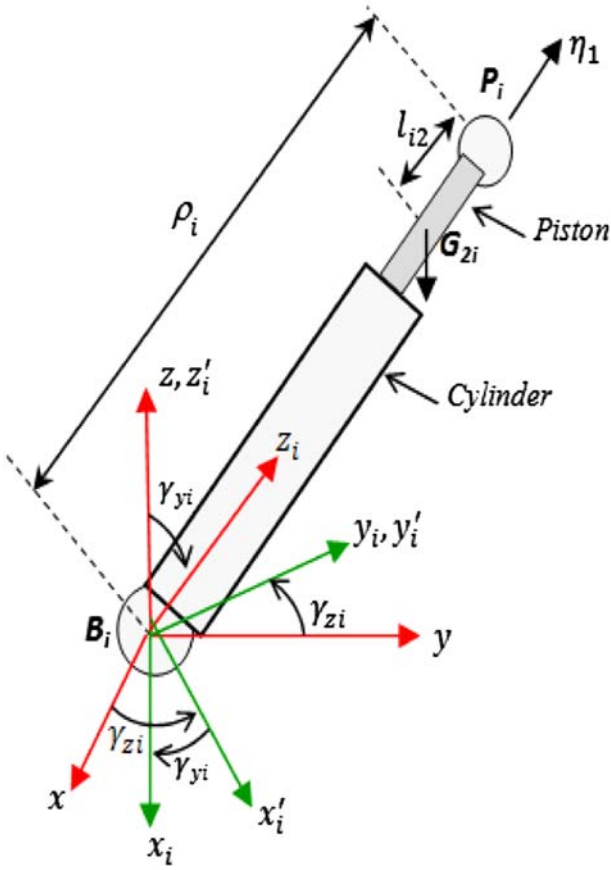

Figure 11. Representation of the *i*th actuator.

$$\dot{\rho}_i = \frac{d\rho_i}{dt} = \overrightarrow{V_{Pi}^T}\ \overrightarrow{\eta_i} \tag{43}$$

$$\overrightarrow{B_iP_i} = \rho_i\ \overrightarrow{\eta_i} \tag{44}$$

$$\frac{d\ \overrightarrow{\eta_i}}{dt} = \frac{d}{dt}\left(\frac{\overrightarrow{B_iP_i}}{\rho_i}\right) = \left[\frac{1}{\rho_i}.\frac{d(\overrightarrow{B_iP_i})}{dt} - \frac{1}{\rho_i^2}.\dot{\rho}_i.\overrightarrow{B_iP_i}\right]$$
$$= -\frac{1}{\rho_i}\left(\overrightarrow{V_{Pi}^T}\ \overrightarrow{\eta_i}\right)\overrightarrow{\eta_i} + \frac{1}{\rho_i}\ \overrightarrow{V_{Pi}} \tag{45}$$

Therefore (substituting (45) into (42), we find:

$$\overrightarrow{v_{G2i}} = \left(1 - \frac{l_{2i}}{\rho_i}\right)\overrightarrow{V_{Pi}} + \frac{l_{2i}}{\rho_i}\left(\overrightarrow{V_{Pi}^T}\ \overrightarrow{\eta_i}\right)\overrightarrow{\eta_i} \tag{46}$$

$$\overrightarrow{v_{G2i}^T} = \left(1 - \frac{l_{2i}}{\rho_i}\right)\overrightarrow{V_{Pi}^T} + \frac{l_{2i}}{\rho_i}\ \overrightarrow{\eta_i^T}\ \overrightarrow{\eta_i^T}\ \overrightarrow{V_{Pi}} \tag{47}$$

- Calculation of V_{Pi} in the frame of the actuator $\{R_s\}$

Let ${}^bR_s$ the matrix of passage of $\{R_s\}$ to $\{R_b\}$ such as:

$${}^bR_s = \begin{bmatrix} c\gamma_{zi}\ c\gamma_{yi} & -s\gamma_{zi} & c\gamma_{zi}\ s\gamma_{yi} \\ s\gamma_{zi}\ c\gamma_{yi} & c\gamma_{zi} & s\gamma_{zi}\ s\gamma_{yi} \\ -s\gamma_{yi} & 0 & c\gamma_{yi} \end{bmatrix} \tag{48}$$

The coordinates of unit vector $\overrightarrow{\eta_i}$ of the axis $\overrightarrow{B_iZ_i}$ in $\{R_s\}$ are $[0\ 0\ 1]^T$, by using the matrix ${}^bR_s$, we obtain:

$$[\overrightarrow{\eta_i}]_b = {}^bR_s \begin{bmatrix} \eta_{xi} \\ \eta_{yi} \\ \eta_{zi} \end{bmatrix}_b = {}^bR_s \begin{bmatrix} 0 \\ 0 \\ 1 \end{bmatrix} = \begin{bmatrix} c\gamma_{zi}\ c\gamma_{yi} \\ s\gamma_{zi}\ c\gamma_{yi} \\ c\gamma_{yi} \end{bmatrix} \tag{49}$$

where $s\gamma_{yi} = \sqrt{\eta_{xi}^2 + \eta_{yi}^2}$, $c\gamma_{yi} = \eta_{zi}$, $s\gamma_{zi} = \frac{\eta_{yi}}{s\gamma_{yi}}$, and $c\gamma_{zi} = \frac{\eta_{xi}}{s\gamma_{yi}}$.We substitute (49) in (48), we find the expression of matrix ${}^bR_s$.

Hence the expression of the $\overrightarrow{V_{Pi}}$ velocity in the reference frame related to the segment is given by:

$$[\overrightarrow{V_{Pi}}]_s = {}^bR_s^T[\overrightarrow{V_{Pi}}]_b \tag{50}$$

- Calculation of the velocity $[\overrightarrow{V_{Pi}}]_b$

$$\frac{d(\overrightarrow{B_iP_i})}{dt} = \frac{d(B_iO_b + O_bO_n + O_nP_i)}{dt} = \frac{d(-{}^bB_i + {}^br + R\,{}^nP_i)}{dt} \tag{51}$$

$$\overrightarrow{V_{P,i}} = \overrightarrow{{}^b\dot{r}} + \dot{R}\ \overrightarrow{O_nP_i} = \overrightarrow{{}^b\dot{r}} + R(\overrightarrow{{}^p\omega_{na}} \wedge \overrightarrow{O_nP_i}) \tag{52}$$

- Determination of ${}^p\omega_{na}$

By applying the velocity composition law, we obtain:

$${}^b\omega_{na} = \begin{bmatrix} 1 \\ 0 \\ 0 \end{bmatrix} \dot{\psi} + R_\theta \begin{bmatrix} 0 \\ 1 \\ 0 \end{bmatrix} \dot{\theta} + R_\psi\ R_\theta \begin{bmatrix} 0 \\ 0 \\ 1 \end{bmatrix} \dot{\phi} \tag{53}$$

$${}^b\omega_{na} = \begin{bmatrix} 1 & 0 & -s\theta \\ 0 & c\psi & s\psi c\theta \\ 0 & s\psi & c\psi c\theta \end{bmatrix} \begin{bmatrix} \dot{\psi} \\ \dot{\theta} \\ \dot{\phi} \end{bmatrix} = M_1 \begin{bmatrix} \dot{\psi} \\ \dot{\theta} \\ \dot{\phi} \end{bmatrix} = M_1\ \Omega \tag{54}$$

The expression of ${}^b\omega_{na}$ in the reference frame related to the mobile plate $\{R_n\}$ is:

$${}^p\omega_{na} = R^T\ {}^b\omega_{na} = R^T\ M_1\ \Omega \tag{55}$$

We substitute (55) in (52), we obtain:

$$\overrightarrow{V_{P,i}} = \overrightarrow{{}^b\dot{r}} - R\ (\overrightarrow{O_nP_i} \wedge \overrightarrow{\omega_{na}}) = \overrightarrow{{}^b\dot{r}} - R\ (\widetilde{P}_i\ R^T\ M_i\ \overrightarrow{\Omega}) \tag{56}$$

$$\overrightarrow{V_{P,i}} = [I_3\ \ -R\widetilde{P}_i\ R^T M_i] \begin{bmatrix} \overrightarrow{{}^b\dot{r}} \\ \overrightarrow{\Omega} \end{bmatrix} = [I_3\ \ -R\widetilde{P}_i\ R^T\ M_i]\dot{X} \tag{57}$$

$$\overrightarrow{V_{P,i}} = [I_3\ \ -R\widetilde{P}_i\ R^T\ M_i]\ J\ \dot{\rho} = J_i\ \dot{\rho}\ \ i = 1, \ldots, 6 \tag{58}$$

where $\overrightarrow{O_nP_i} = \begin{bmatrix} r_n\ cos(\beta_i) \\ r_n\ sin(\beta_i) \\ 0 \end{bmatrix} = \begin{bmatrix} P_{xi} \\ P_{yi} \\ P_{zi} \end{bmatrix}$ and $\tilde{P} = \begin{pmatrix} 0 & -P_{zi} & P_{yi} \\ P_{zi} & 0 & -P_{xi} \\ -P_{zi} & P_{yi} & 0 \end{pmatrix} = \begin{pmatrix} 0 & 0 & P_{yi} \\ 0 & 0 & -P_{xi} \\ -P_{zi} & P_{yi} & 0 \end{pmatrix}$

- Calculation of $\omega_{a,i}$ in the reference frame related to the actuator $\{R_s\}$

The velocity of rotation of the actuator in $\{R_s\}$ is given by:

$$\overrightarrow{\omega_{a,i}} = \frac{1}{\rho_i} \begin{bmatrix} V_{Pxi} \\ V_{Pyi} \\ 0 \end{bmatrix}_s = \frac{1}{\rho_i} \begin{bmatrix} 1 & 0 & 0 \\ 0 & 1 & 0 \\ 0 & 0 & 0 \end{bmatrix} {}^bR_s^T\ [\overrightarrow{V_{Pi}}]_b = D_i[\overrightarrow{V_{Pi}}]_b \tag{59}$$

Hence:

$$\overrightarrow{\omega_{a,i}^T} = [\overrightarrow{V_{Pi}^T}]_b\ D_i^T \tag{60}$$

We substitute (46), (47), (59), and (60) in (40), we obtain after development:

$$T_{pis,i} = \frac{1}{2} \left[\overrightarrow{V_{Pi}^T}\ m_{pis,i} \left(1 - \frac{l_{i2}}{\rho_i}\right)^2 \overrightarrow{V_{Pi}} + \dot{\rho}\ \frac{l_{i2}}{\rho_i} \left(2 - \frac{l_{i2}}{\rho_i}\right) \dot{\rho}_i + \overrightarrow{V_{Pi}^T}\ D_i^T\ I_{pis,i}\ D_i\ \overrightarrow{V_{Pi}} \right] \tag{61}$$

Calculation of the kinetic energy of each cylinder

The cylinder fixed at the B_i point has only a rotational movement, so only a kinetic energy in rotation:

$$T_{\text{cyl},i} = \frac{1}{2}\ \omega_{a,i}^T\ I_{\text{cyl},i} \omega_{a,i} = \frac{1}{2}\ \overrightarrow{V_{Pi}^T}\ I_{\text{cyl},i} D_i\ \overrightarrow{V_{Pi}} \tag{62}$$

Calculation of the kinetic energy of each actuator

$$T_{a,i} = T_{cyl,i} + T_{pis,i} = \frac{1}{2} \left[\overrightarrow{V_{Pi}^T}\ a_i\ \overrightarrow{V_{Pi}} + \dot{\rho}\ b_i\ \dot{\rho}_i + \overrightarrow{V_{Pi}^T}\ c_i\ \overrightarrow{V_{Pi}} \right] \tag{63}$$

where $a_i = m_{pis,i}(1 - \frac{l_{i2}}{\rho_i})^2$, $b_i = \frac{l_{i2}}{\rho_i}\left(2 - \frac{l_{i2}}{\rho_i}\right)$, and $c_i = D_i^T\ (I_{pis,i} + I_{cyl,i})\ D_i$.
For the six actuators:

$$T_{a,i} = \frac{1}{2}\ \dot{\rho}^T \left[\sum_{i=1}^{6} J_i^T\ a_i\ J_i + \ b_i\ I_{6x6}\ +\ J_i^T c_i J_i \right] \dot{\rho} \tag{64}$$

Hence the inertia matrix of the six actuators is given by:

$$I_a = \sum_{i=1}^{6} (J_i^T \; a_i \, J_i + \; b_i \, I_{6x6} \; + \; J_i^T c_i J_i) \tag{65}$$

Kinetic energy of the mobile plate

$$\begin{aligned} T_p &= \frac{1}{2} \; {}^b\dot{r} \; m_{na} \; {}^b\dot{r} \; + \; \frac{1}{2} \; {}^p\omega_{na}^T \; I_{na} \; {}^p\omega_{na} \\ &= \frac{1}{2} \; {}^b\dot{r} \; m_{na} \; {}^b\dot{r} \; + \; \frac{1}{2} \; \Omega^T \; R \; M_1^T \; I_{na} R^T \; M_1 \Omega \end{aligned} \tag{66}$$

$$T_p = \frac{1}{2} \; \dot{X}^T \begin{bmatrix} M_p & 0 \\ 0 & I_p \end{bmatrix} \dot{X} = \frac{1}{2} \; \dot{\rho}^T \left(\; J^T \begin{bmatrix} M_p & 0 \\ 0 & I_p \end{bmatrix} J \; \right) \dot{\rho} \tag{67}$$

where ${}^p\omega_{na}$: the velocity of rotation of the mobile plate expressed in R_n. $I_p = R \; M_1^T \; {I_{na}}^T \; M_1$: tensor of inertia of the mobile plate, and $I_{na} = diag(I_{xx}, I_{yy}, I_{zz})$

Appendix B. General Principle of SPEA-II

The SPEA-II algorithm proposed by Zitzler et al. [9] differs from its predecessor the SPEA by a size of the fixed archive and a calculation of the performance of the individuals more refined. Moreover, only the individuals of the archive take part in the process of reproduction. The principal characteristics of this algorithm are:

- The quality of an individual is judged according to criteria of domination in the global population. More precisely, we affect to each individual i a value $S(i)$, that represents the number of the individuals of the population which are dominated by i., the quality of the individual j is then obtained by adding the $S(i)$ for all the individuals i that dominate j.
- The estimation of the density is effected by a method inspired on that of nearest neighboring: the distances to all neighboring are calculated, and we add to the quality of the individuals (described in the preceding paragraph) the inverse of the distance to the $k^{i\text{th}}$ neighboring (generally k is fixed to 1).
- The algorithm uses an archive of individuals of fixed size. In case of necessity, the sorting of the archive is done by removing the individual which has the nearest neighboring (in case of equality, we look at the second nearest neighboring).

The principle of SPEA-II is clarified by the following algorithm:

- The inputs of the algorithm are: N : population size, $\overline{N}$: archive size, and T: maximum number of generations.
- The output of the algorithm is: A: the nondominated set.
- The steps of the algorithm are:

Step 1: *Initialisation*, generate an initial population P_0 and create the empty archive $\overline{P_0}$ set $t = 0$.
Step 2: *Fitness assignment*: Calculate fitness values of individuals in P_t and $\overline{P_t}$.
Step 3: *Environmental selection*: Copy all nondominated individuals in P_t and $\overline{P_t}$ to $\overline{P}_{t+1}$. If size of $\overline{P}_{t+1}$ exceeds $\overline{N}$ then reduce $\overline{P}_{t+1}$ by means of the truncation operator, otherwise if size of $\overline{P}_{t+1}$ is less than $\overline{N}$ then fill $\overline{P}_{t+1}$ with dominated individuals in P_t and $\overline{P_t}$.
Step 4: *Termination*: If $t \geq T$ or another stopping criterion is satisfied then set A to the set of decision vectors represented by the nondominated individuals in $\overline{P}_{t+1}$. Stop.
Step 5: *Mating selection*: Perform binary tournament selection with replacement on $\overline{P}_{t+1}$ in order to fill the mating pool.

About the Authors

Ridha Kelaiaia received the diploma of engineer on mechanical engineering from Guelma University in 1996. He also received the diploma of magister in robotics from the Military polytechnic school, Algiers, in 2004. And a PhD degree in electromechanical engineering (robotics) from Skikda University, Algeria in 2012. His research interests include design, modeling, and optimization of parallel kinematics machines.

Olivier Company received a MS degree in mechanical engineering from the Arts et Métiers School in Paris, France in 1995 and a PhD degree in automatic control from the University of Montpellier, France in 2000. He is with the LIRMM since 2001. His current position is an associate professor in robotics for the University of Montpellier. He working on design and modeling of parallel kinematics machines.

Abdelouahab Zaatri was born in 1955 in Algéria. He received the diploma of engineer on electricity from the University of Louvain at Louvain la Neuve, Belgium in 1981. He, also, received the PhD in robotics from the Katholieke Universiteit van Leuven, Belgium, in 2000. He worked as an engineer at the Algerian electrical company named: "Sonelgaz" since 1981–1989. He worked from 1993 to 1995 and since 2000 as a lecturer at the University of Constantine at the department of Mechanics. He has published some books on various technological fields such as operations research, system control, learning Java, and automation. His research interests are oriented towards robotics, automation, renewable energies, and bio-robotics. He is actually the head of the Laboratory of Advanced Technology Applications at the University of Constantine and he is the head of the robotics team at the laboratory of mechanics at the University of Constantine.